Aerospace Science and Technology 100 (2020) 105786

Contents lists available at ScienceDirect

Aerospace Science and Technology

www.elsevier.com/locate/aescte

Effect of fuel-jet injection angle variation on the overall performance of a SCRAMJET engine

Vatsalya Sharma [a], Vinayak Eswaran [a,*], Debasis Chakraborty [b]

[a] Department of Mechanical and Aerospace Engineering, Indian Institute of Technology Hyderabad, India
[b] Department of Aerospace Engineering, Indian Institute of Technology Bombay, India

ARTICLE INFO

Article history:
Received 9 February 2020
Received in revised form 11 February 2020
Accepted 15 February 2020
Available online 25 February 2020
Communicated by Suresh Menon

Keywords:
SCRAMJET engine
RANS
Transverse sonic injection
Supersonic crossflow
Shock augment mixing

ABSTRACT

Air-fuel mixing in a SCRAMJET engine is augmented by the interaction of the transverse fuel jet with the incoming supersonic air. The strong bow shock created by this interaction aids in mixing and increases the fuel residence time, but it also leads to loss in performance of the SCRAMJET engine through the loss of stagnation pressure, and rise in entropy in the combustor. One of the ways to address this issue is to weaken the bow shock by changing the angle of injection of fuel into the combustor. In the present study, the effect of variation of the injection angle, measured in the direction of the cross-flow from a line perpendicular to it (and the wall), has been numerically studied and analyzed on a 3-D SCRAMJET combustor of generic design with dual injectors, using Menter's SST model for turbulence on an in-house 3-D unstructured grid RANS solver. The angle for each injector is independently varied between 0° and 45° with an increment of 15°, while the jet positions are kept fixed at locations previously found to be optimum for the chosen flow conditions and zero angle (i.e. transverse) injection. It is observed that in every case that positive non-zero angles of injection, in the direction of the crossflow, increase thermodynamic efficiency, while the negative non-zero angles, opposing the crossflow, augment mixing. As mixing is of paramount importance in the SCRAMJET engine, due to high speeds and low residence times, we conclude that the best option is to have the angle of fuel jet injection in the direction opposing the incoming flow – a recommendation that has not been seen yet in the research literature. The degree to which the injection is slanted towards the incoming flow can be decided on the basis of the desired rate of the simultaneous penetration of the fuel into the recirculating flame-holder, which increases with increasing angle.

1. Introduction

The high thrust required for sustained supersonic and hypersonic flights can be fulfilled by using SCRAMJET (supersonic ramjet) engines of relatively simple design with no moving parts [1,2]. One of the challenges in the design of the SCRAMJET engines is to ensure rapid mixing between the air and the fuel which is necessitated by the short residence time (which is of the order of several milliseconds) of the incoming air. One way to increase the residence time in a combustor is to inject the fuel jet in the transverse direction at sonic speed in a supersonic cross-flow, which is a configuration that has been studied extensively by the researchers [3–8] and results in a simple and reliable design.

A major design challenge in the SCRAMJET engines is to hold, stabilize and sustain flame in the combustor for continuous combustion. One of the simplest designs capable of flame holding and stabilization is to have a combustor with the injectors placed downstream of a backward facing step [9–13]. The step creates a large recirculation zone which, with the hot gases contained therein, serves as a continuous ignition zone.

The study of air-fuel mixing is of critical importance, as good air-fuel mixing in the combustor would result in good combustion, while bad mixing may not even result in combustion. It has been further reported in the literature [14–16] that the mixing of the jet and the incoming flow is decoupled from combustion due to the very strong baroclinic torque that is produced in the flow field due to interaction of the transverse jet with the incoming supersonic air. This shock augmented mixing of the air-fuel streams is not significantly affected by the heat release due to the combustion in the supersonic flow field. Therefore, cold flow analysis of the flow field could be used, at least as a first approximation, to optimize the design of a SCRAMJET engine based on mixing considerations alone.

* Corresponding author.
E-mail address: eswar@iith.ac.in (V. Eswaran).

https://doi.org/10.1016/j.ast.2020.105786
1270-9638/

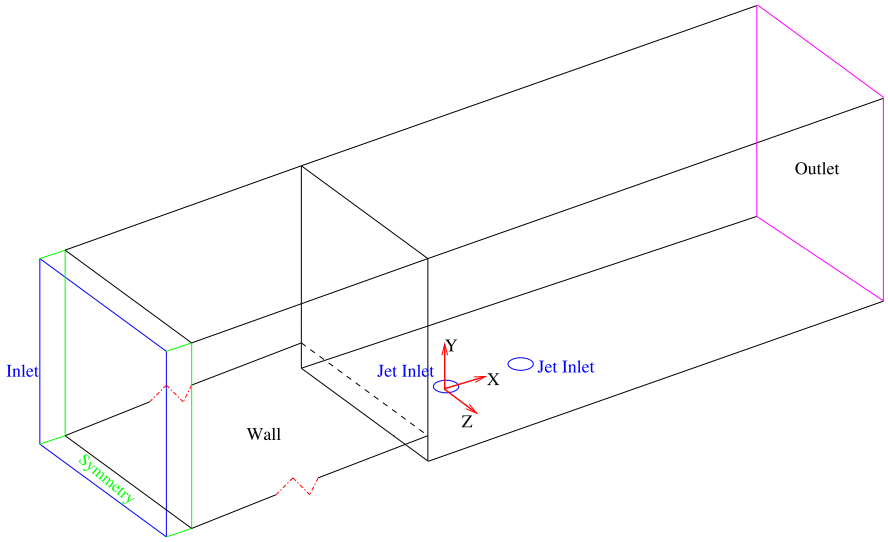

Fig. 1. Isometric view of the domain. (For interpretation of the colors in the figure(s), the reader is referred to the web version of this article.)

The overall performance of the SCRAMJET engine depends on a wide range of geometrical parameters such as the location and orientation of the injector, the angle of injection and the spacing between the injectors, etc. By optimizing the aforementioned parameters, better performance can be extracted [17,18]. The SCRAMJET geometry given by McDaniel et al. [9,10] is used in this study. Previous studies of the same configuration by the present authors have established the optimal location for one and two injectors for strictly lateral fuel jet injections [17,18] and also the effect of the isolator length before the inlet of the combustor [17,18]. In this paper we study the effect of the variation in the injector angles on the performance of the combustor.

Several researchers [19–21] have found that slanting the angle of injection towards the downstream of the crossflow weakens the bow shock at the injector, and leads to a lower pressure loss near the injector. An experimental study on the effect of the angle of injection with three different injector shapes was conducted by Gruber et al. [22]. They concluded that the injector shape does not substantially affect the transverse jet flow field but varying the angle of injection has dramatic effects. Jeong et al. [23] performed experiments on the variation of the angle of injection with combustion in a cavity-based setup. Wang et al. [24] computationally studied the variation of the angle for transverse sonic injection in the cavity and reported results similar to the experiments [23]. Huang et al. [25] used RANS models to study the effect of the injection angle at different injector-to-free stream pressure ratios on a 2D configuration. Zang et al. [26] used a hybrid RANS-LES model along with experiments to study the turbulent structures in the flow.

It should be noted that all the aforementioned studies have been done on a simple geometry of a flat plate with a single injector, whereas a working SCRAMJET engine has multiple injectors along with a flame holder. In the best knowledge of the present authors, the effect of variation of the angle of injection with multiple injectors and a flame holder has not been systematically studied in the literature. Therefore the aim of this study is to study a range of angles of injection for a two-injector configuration of a SCRAMJET engine with a backward facing step flame-holder with the aim of optimizing performance.

2. Numerical method

The study is conducted using an in-house parallel three-dimensional unstructured grid RANS solver developed by the authors [27,18,17]. A low-speed preconditioned form of the Navier-Stokes equation [28] is used in the solver. The convective term of the Navier-Stoke's equation is modeled using the 2nd order Roe scheme [29] which has been preconditioned for low speeds [30] along with the Venkatkrishnan limiter [31,32]. The Green-Gauss cell based method is used to compute the gradients in the governing equations. In order to march the solution to steady-state, explicit time-stepping using 4th order Runge-Kutta method [33] has been implemented. The SST k-ω two-equation model of Menter [34] in its low Reynolds number form is used to model turbulence. Laminar and turbulent Prandtl numbers are taken as 0.71 and 0.9 respectively. In order to track mixing of the injected jet with the main air flow, a convection-diffusion equation is solved for a passive scalar ϕ the *"mixing fraction"* coupled with the system of governing equations. The value of the turbulent Schmidt number (Sc_t) is fixed as 0.9. The value of ϕ at a point in the flow will indicate the amount of mixing of the fuel and air streams, say $\phi = 0.8$ indicates a 80% fuel stream and 20% air stream mixture (by mass). In practice, the fuel stream would be, say a kerosene-air mixture, which for convenience we take in this study to have the same properties as air. Further details about the governing equations and their implementation can be found in Sharma et al. [27,18,17].

3. Numerical validation and verification of the solver

The RANS solver is validated for benchmark cases to establish its capabilities and accuracy in the following sub-section. These validations and grid independence study were done extensively in previous papers [18,17] and are briefly summarized here for the purpose of readability.

3.1. Transverse dual sonic injection in supersonic cross flow over backward facing step

Experimental results obtained using Laser Induced Iodine Fluorescence (LIIF) by McDaniel et al. [9] to study the penetration and spread of dual staged transverse sonic jet in a supersonic cross flow over a backward facing step have been used as a validation test case for our solver. The 3-D isometric view of the computational domain along with boundary section names is shown in Fig. 1. Fig. 2 shows the 2-D views in the planes parallel and normal to the injectors, with the required dimensions given in Table 1.

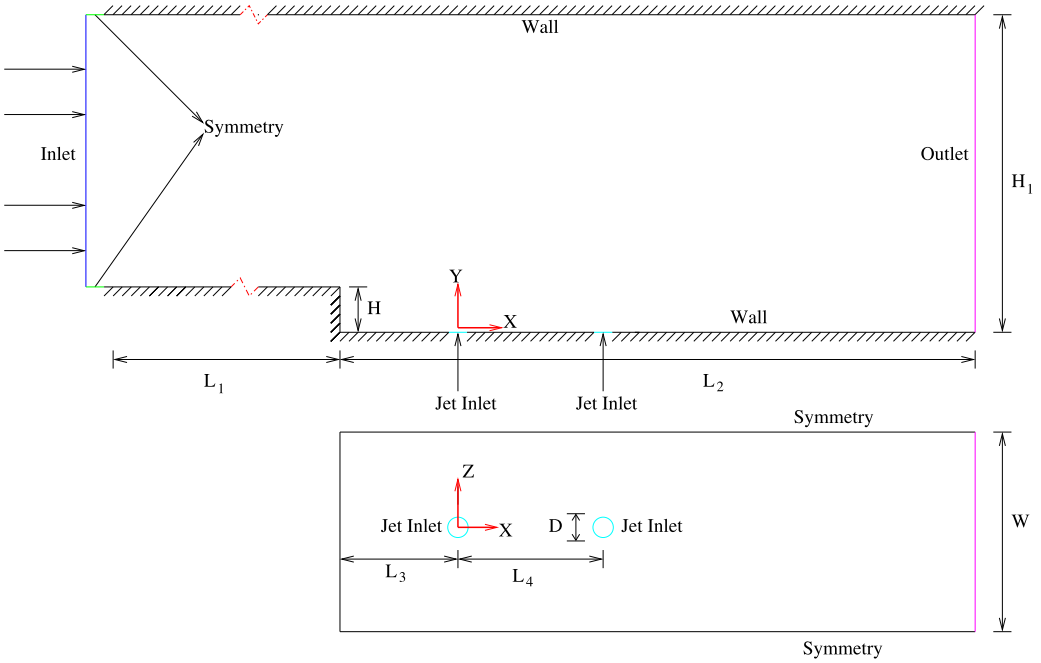

Fig. 2. Geometry for simulations and its boundary conditions.

Table 1
Domain dimensions.

Parameter	Value
Injector diameter (D)	1.93 mm
Leading injector location	0, 0, 0
L_1	$56.0D$
L_2	$31.0D$
L_3	$4.94D$
L_4	$6.6D$
W	$31.0D$
H	$15.8D$
Step location	$-4.94D$

Note a line break has been used in the length of L_1 to fit the image.

Meshes were made using the ICEM-CFD software in CGNS format. Unstructured 3-D meshes with quadrilateral elements at the boundary section and hexahedral elements in the inner computational section have been used. Since SST is a low Reynold's number model, $y^+ < 1$ is required for all the grids near the wall.

3.2. Placement of the two jets

The two jets are located at $L_3 = 4.94D$ and $L_4 = 6.6D$, which has been determined as the optimal locations in the previous papers [17,18] for the chosen flow conditions with 0 angle (i.e. normal to the wall) injection. These locations will be kept fixed in all the simulations of the present study, with only the jet injection angles, but not the jet positions, being varied.

3.3. Boundary conditions

At the inlet, for a free-stream Mach number (M_∞) of 2.05 and pressure inlet boundary condition were prescribed, with total pressure (P_0) = 274000 Pa, static temperature (T_{static}) = 163 K and total temperature (T_0) of 250 K. The wall is assumed as adiabatic, so $\mathbf{U} = 0$, $\frac{\partial T}{\partial n} = 0$, $\frac{\partial P}{\partial n} = 0$, $\frac{\partial \tilde{\nu}}{\partial n} = 0$ are prescribed as boundary conditions there. At outflow, $\frac{P_0}{P_\infty} = 1$ is prescribed, the remaining quantities were taken from interior values. For all the sections labeled as symmetry, $\frac{\partial \mathbf{Q}}{\partial n} = 0$ is prescribed. Since the injection is done at sonic speed, choked flow conditions are prescribed at the jet inlets. Inlet jet dynamic pressure ratio (Q) is given as:

$$Q = \frac{1}{M_\infty^2}\frac{P_{jet}}{P_\infty} \tag{1}$$

where P_{jet} is the injected jet static pressure and P_∞ is the free stream static pressure. Simulations were performed for Q = 1.05. Boundary conditions for the turbulent variables and for the passive scalar are given in Table 2. For calculating the value of the turbulent kinetic energy k and the specific dissipation ω at the inlet, the value of turbulence intensity (I) is used with the following formulae:

$$k = 1.5I^2U_{inlet}^2 \tag{2}$$

$$\epsilon = C_\mu^{3/4}k^{3/2}l^{-1} \tag{3}$$

$$\omega = \frac{k}{C_\mu \epsilon} \tag{4}$$

where I is the level of turbulence intensity, U_{inlet} is the inlet velocity, l is length scale given as $l = 0.07L$, where L is characteristic length of domain. The value of I is taken as 5% for all the simulations.

Table 2
Boundary conditions for turbulence variables and passive scalar.

Section name	SST boundary condition	Scalar (ϕ) boundary conditions
Inlet	$I = 5\%$	$\phi = 0$
Adiabatic wall	$k = 0$ $\omega = 0$	$\phi = 0$
Outlet	$\frac{\partial k}{\partial n} = 0$ $\frac{\partial \omega}{\partial n} = 0$	$\frac{\partial \phi}{\partial n} = 0$
Symmetry	$\frac{\partial k}{\partial n} = 0$ $\frac{\partial \omega}{\partial n} = 0$	$\frac{\partial \phi}{\partial n} = 0$
Transverse jet inlet	$\frac{\partial k}{\partial n} = 0$ $\frac{\partial \omega}{\partial n} = 0$	$\phi = 1$

3.4. Grid independence study

The grid sensitivity study [17,18] was done with three grids of size $N_1 = 3256500$, $N_2 = 399822$ and $N_3 = 48291$ using the Grid

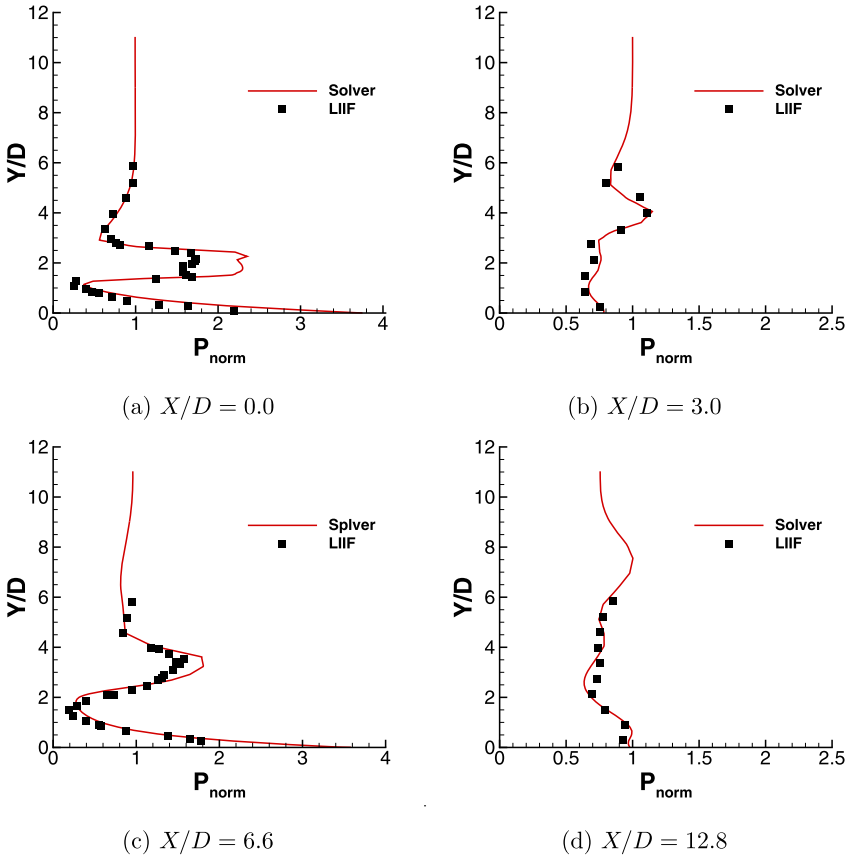

Fig. 3. Comparison of P_{norm} profile at different X/D against LIIF experiments done by McDaniel et al. [10].

Convergence Index (GCI) [35]. The solution was computed on all 3 grids, and value of jet penetration were compared. The jet penetration determined by the distance of the passive scalar contours of ϕ = 1% from the bottom wall on the X-Y mid plane of the domain. On the finest grid, average order of accuracy p_{avg} was obtained around 2.248 and maximum GCI (i.e. the maximum uncertainty in the computed jet penetration value) was obtained as 2.047%. On the basis of GCI, the 3D grid with 3256500 hexahedral cells was chosen [17,18] and also used for the computations in the present paper.

3.5. Comparison against experimental data

The results [17,18] on the finest mesh were compared with the experiments of McDaniel et al. [10]. P_{norm} and U_{norm} defined by Eq. (5) and (6) respectively, have been plotted here and shown in Figs. 3 and 4 respectively, for different locations at the mid X-Y plane. A good match is obtained. Hence, the solver has been successfully validated with the required grid independence study.

$$P_{norm} = \frac{P}{P_{\infty}} \tag{5}$$

$$U_{norm} = \frac{U_x}{U_{x,\infty}} \tag{6}$$

3.6. Convergence criteria

In the previous [17,18] and the present computations, mesh division for parallel processing were done using METIS for MPI based parallel simulations. Explicit time stepping with CFL numbers ranging from $0.1 - 0.4$ are taken for the simulations. At all the CFL numbers between $0.1 - 0.4$, same steady-state P_{norm} profile is achieved, showing a good temporal convergence. The solution is considered converged once the normalized velocity and pressure residuals are below $1e^{-6}$ and turbulent variables' residuals below $1e^{-3}$.

4. Results

In order to better understand the results of the simulations to follow, we will briefly review the major features of the flow as found in the previous works [17,18].

4.1. Major features of the flow

Key features of the flow-field with two fuel injectors is been shown are Fig. 5. The figure consists of two parts. In the first part of the figure, the P_{norm} isobars are plotted with the Mach number contours, whereas in the lower part, the contours of mixing fraction ϕ with streamlines are shown. The plots are of the mid-X-Y plane of the combustor.

It is observed from the figures that the flow from the inlet encounters the backward facing step, over which the turbulent boundary layer separates and forms a shear layer. As a result, a recirculation zone is formed behind the step and the flow expands through formation of a Prandtl-Meyer Expansion Fan (PMEF) above it. The fuel is injected in the transverse direction at the sonic speed into the combustor from the two injectors in the downstream of the step, as shown in Fig. 2. It should be noted that both the injectors are exactly same in dimensions and mass flow-rate, at the sonic conditions. When the air stream encounters the under-expanded jet from the first injector, a strong bow shock is created, with a small upstream separation bubble. A region of strong lateral convection near the first injector is created by the interaction of the shock-waves generated by the jet and the PMEFs at the step.

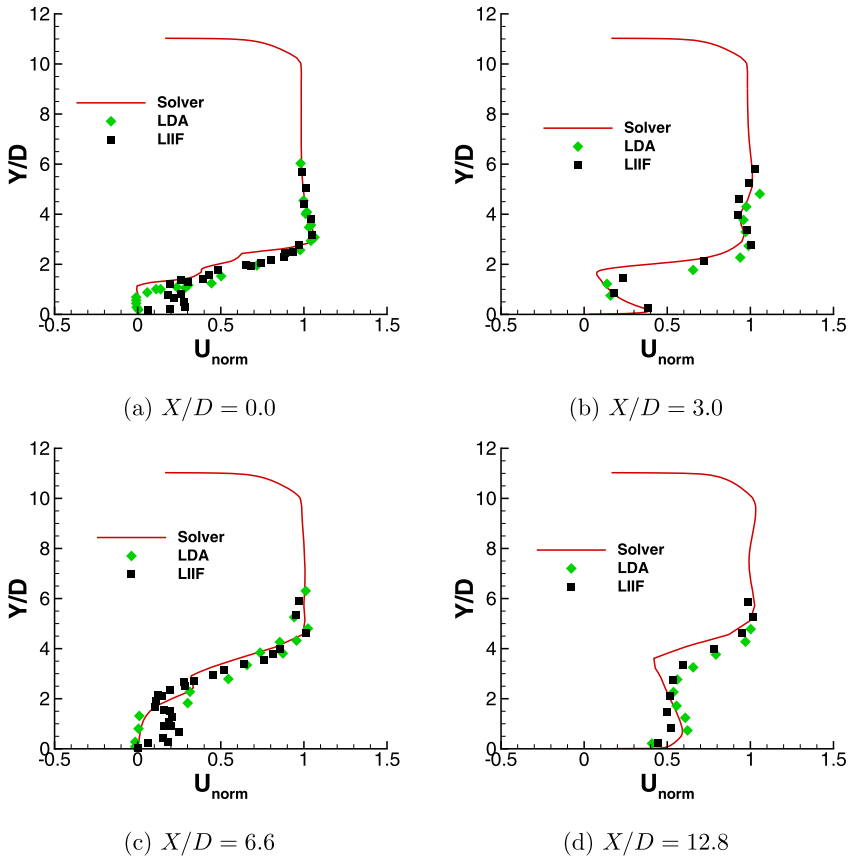

Fig. 4. Comparison of U_{norm} profile at different X/D against experiments done by McDaniel et al. [10].

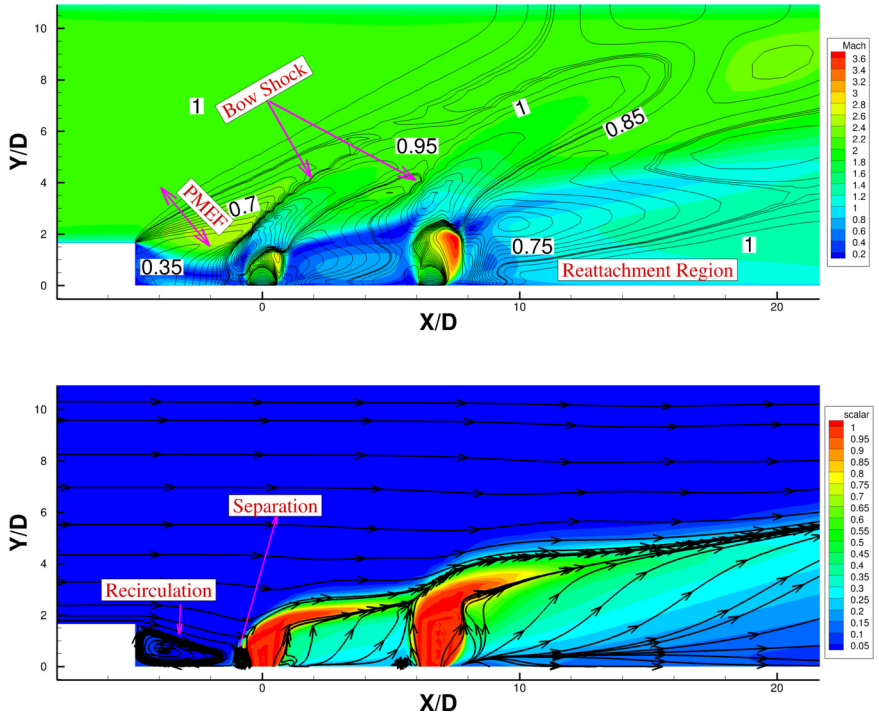

Fig. 5. Top: center-plane P_{norm} isobars with Mach number contours. Bottom: Mass fraction of scalar with stream lines.

This interaction of the strong bow shock with the fuel jet leads to the creation of baroclinic torque, which then results in the formation of a counter-rotating vortex pair in the streamwise direction after the jet inlet. The incoming high speed air resists the upwards penetration of the jet. This is termed as the blockage effect, which bends and elongates the jet in the streamwise direction, as seen in Fig. 5. The bow shock from the second jet is weaker than at the leading jet, as can be seen by comparing flow expansions from

Fig. 3a and 3c. Multiple injectors increase the mass fraction of fuel in the combustor and raise the mixing boundary as seen in Fig. 5. Due to absence of any flow accelerating mechanism downstream of the injector, the mixing boundary decelerates and then decays. In the far-field region the flow reattaches to the surface and again renormalizes to $P_{norm} = 1$ through reattachment shocks.

4.2. Methodology

The present aim is to study the effect of the injection angles on the flow and performance of the combustor. The injection angle is the angle made by the injected jet direction with the vertical Y-direction, towards the X-direction, i.e., the direction of the crossflow. The angle of injection is varied for the two injectors, in various combinations, to study its effects on the overall performance of the SCRAMJET engine. Therefore a completely transverse injection (as solved in Sec. 3) will have a 0° angle of injection. The case with dual transverse sonic injections in the Sec. 3.1 will be referred to as the *baseline case*. As mentioned earlier, the locations of the two jets will be kept fixed at $L_3 = 4.94D$ and $L_4 = 6.6D$ and only the jet injection angles will be varied in the study. The angle of both the injectors is varied to a maximum of 45°, in the step increment of 15°. Following the premise with Sharma et al. [17,18], in order to quantify mixing, the effect of streamwise vorticity along with jet penetration and spread will be evaluated. To evaluate performance, the loss of stagnation pressure and rise in entropy of the system has been evaluated using the definitions described in the references [17,18] and in the following sub-sections.

4.2.1. Effect of streamwise vorticity

Mixing of air-fuel streams in the SCRAMJET combustor is augmented by strong streamwise vorticity in the flow field. When an under-expanded jet at sonic speed is injected in the transverse direction to the incoming flow, it creates a complex flow-field as described in detail by Sharma et al. [27]. A transverse sonic jet creates strong pressure gradients through bow and oblique shocks in a high speed compressible flow, resulting in this baroclinic torque, which in turn creates streamwise vorticity downstream. In order to assess the effect of streamwise vorticity on the mixing and the flowfield, the average *magnitude* of the streamwise vorticity ($\Gamma(x)$) is computed in the Y-Z plane of the flow domain which is computed as:

$$\Gamma(x) = \iint_{yz} \left| \frac{\partial v}{\partial z} - \frac{\partial w}{\partial y} \right| dydz \tag{7}$$

Higher values of $\Gamma(x)$ implies a stronger streamwise vorticity and a higher lateral momentum of the jet in the computational domain.

4.2.2. Mixing characteristics

The injected jet is tracked in the combustor using the passive scalar ϕ described in Sec. 2. The ϕ value thereby varies between 0 and 1, where 0 represents pure air stream and 1 represents pure fuel-jet stream. Various mixing characteristics like jet penetration and spread are plotted, to quantify the extent of mixing of air-fuel stream. The jet penetration is obtained by extracting ϕ = 1% of the injected value on the X-Y mid-plane of the domain. Similarly, the jet spread is obtained by determining the horizontal distance between two $\phi = 1\%$ contours at $Y = D$ on the Y-Z plane at each X location. By measuring the penetration and spread the extent of the mixing boundary can be studied.

Fig. 6 shows the 3-D region in the computational domain where ϕ is greater than 1%. This region is known as the volume of mixing, which has been computed for all the cases. The volume of mixing, along with the data on jet penetration and spread, completes the overall quantification of the air-fuel mixing in the computational domain.

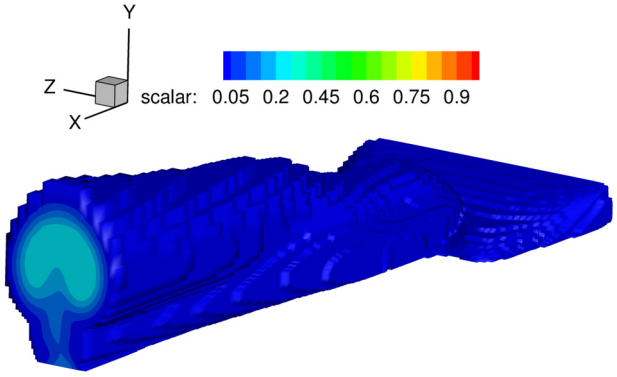

Fig. 6. Volume of air-fuel mixing in the computational domain.

4.2.3. Stagnation pressure

Stagnation pressure at a point in the flow is given by:

$$P_0 = \frac{1}{2}\rho \mathbf{V}^2 + P \tag{8}$$

where P_0 is the stagnation pressure and P is the static pressure. A high exit velocity is required to obtain high thrust, and from Eq. (8), it can be seen that the amount of kinetic energy that can be extracted from the flow is directly related to the stagnation pressure P_0 distribution. Therefore, it is important to avoid loss in stagnation pressure (P_0) since it directly results in loss of thrust. SCRAMJET configurations with transverse sonic jets produce substantial loss in stagnation pressure, although this is compensated by better mixing achieved by the jet. In order to characterize the performance as a function of loss in stagnation pressure, P_0 is plotted as the mass flow weighted average in the Y-Z plane at different X values, which is given by:

$$P_0(x) = \iint_{yz} P_0 \rho u \, dy \, dz \Big/ \iint_{yz} \rho u \, dy \, dz \tag{9}$$

and then subsequently normalized as $P_{0,norm}$ by dividing $P_0(x)$ with the P_0 value prescribed at the inlet.

4.2.4. Rise in entropy

An irreversible process leads to increase in the entropy of a system. The rise in entropy relates to the total amount of energy unavailable to do work. Hence a greater rise in entropy results in a less efficient system. Entropy increase (ΔS) in the SCRAMJET combustor rises primarily due to the mixing of the jet and air and due to presence of shocks in the system. The change in entropy in the computational domain at every cell center c is computed using Gibb's law as:

$$\Delta S_c = C_p \, ln(T_{norm}) - R \, ln(P_{norm}) \tag{10}$$

where the reference state is taken as the inlet condition. The entropy in the Y-Z plane is then evaluated as a mass flow weighted average:

$$\Delta S(x) = \iint_{yz} \Delta S_c \rho u \, dy \, dz \Big/ \iint_{yz} \rho u \, dy \, dz \tag{11}$$

In order to study and analyze the effect of varying angle of injection (α) on the overall performance of the SCRAMJET engine,

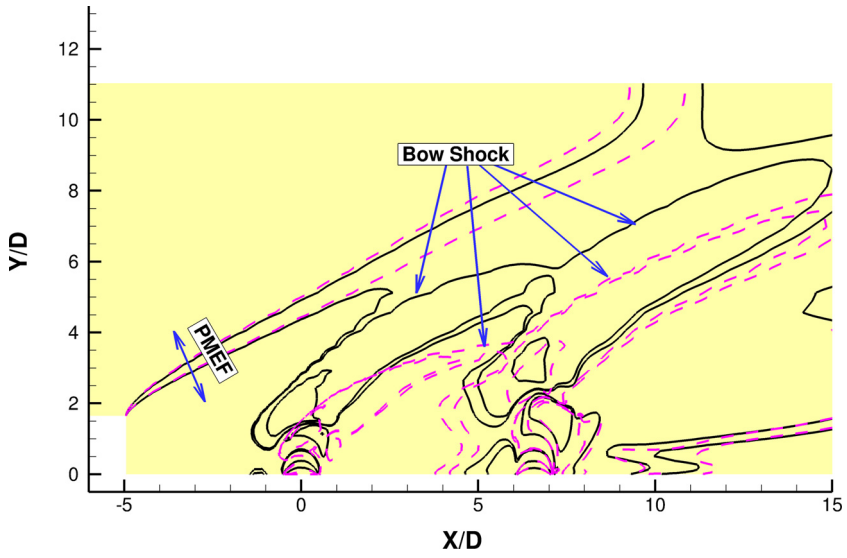

Fig. 7. Superposition of the isobars $P_{0,norm}$ of the baseline case (solid lines) and the case A1c (dashed lines).

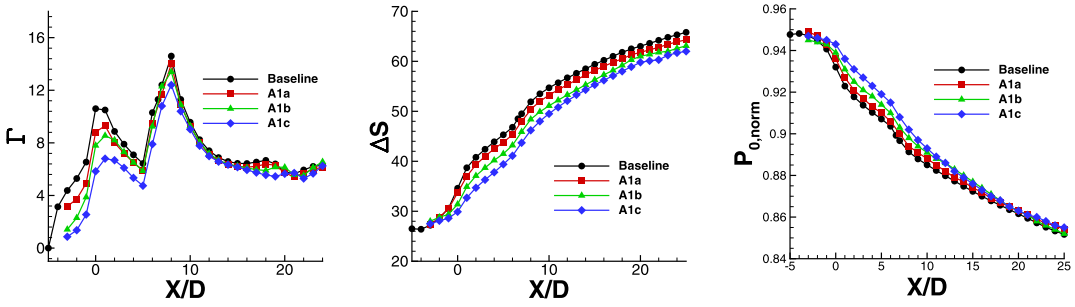

(a) Effect of Streamwise Vorticity (b) Entropy (c) Stagnation Pressure

Fig. 8. Flow characteristics for Case A1.

a number of simulations have been performed by varying α in different combinations. The simulations are broadly classified into two cases. In the first case, the α is varied from 0° to 45° making the jets inject the fuel slanted into the streamwise direction of the incoming flow. In the second case, the α is varied from 0° to −45° to make the jets inject the fuel slanted in the direction opposite to the flow from the inlet. The results obtained in Sec. 3.1 shall be referred to as the baseline case. All the results have been compared against the baseline case, which helps in obtaining a clear understanding their effect on the performance of the SCRAMJET engine. With reference to Fig. 1 it should be noted that the origin of the X-Y-Z coordinate system is located at the center of the 1*st* jet and $X = 6.6D$ is the position of the 2nd jet in all the figures and cases that follow.

4.3. Case A: α variation between 0° and 45°

The angle of injection of the jets in this case is changed from the transverse direction into the streamwise direction of the incoming cross-flow. In this case, the α of the injectors is varied between 0° and 45°. This variation of α results in different combinations of injector angles which are grouped into various sub-cases. The section ends with comparison of the flow features between the different sub-cases and the baseline case.

4.3.1. Case A1

In Case A1, the angle of injection (α) for the first injector is varied, while the α of the second injector is maintained at 0°. The different configurations studied in this case are listed in Table 3.

Table 3
Case A1.

Section name	A1a	A1b	A1c
Injector 1	15°	30°	45°
Injector 2	0°	0°	0°

Fig. 7 shows the imposition of the isobars of Case A1c with the baseline case, while Figs. 8 and 9 show the comparison of the various flow properties for Case A1. A change in the structure of the bow shock from the 1*st* injector can be noted in the figure, with the changes in α. Even with this change, 1*st* bow shock continues to impinge upon the 2nd bow shock, which also undergoes some changes in the shock structure, although the α of the latter remains unchanged. Increasing the α of the first jet decreases the transverse momentum while increasing its streamwise momentum. An immediate effect of increasing the α for the first injector can be clearly seen in the decrease of the peak values of Γ_x at the first injector ($X \approx 0$) in Fig. 8a. This decrease shows the counter-rotating vortices (CRV), that are generated near the injector and are responsible for mixing, have become weaker than in the baseline case. The increase in the streamwise momentum of the jet also does not allow the CRV to rise as much as in the baseline case, so Γ_x remains lower after the first injector, causing a lower peak even at the second injector ($X \approx 8$). The decrease in the transverse momentum further results in an overall decrease in the penetration height and spread between the injectors, with the high-speed incoming flow bending the streamlines from the injectors to align them more in the direction of the streamwise

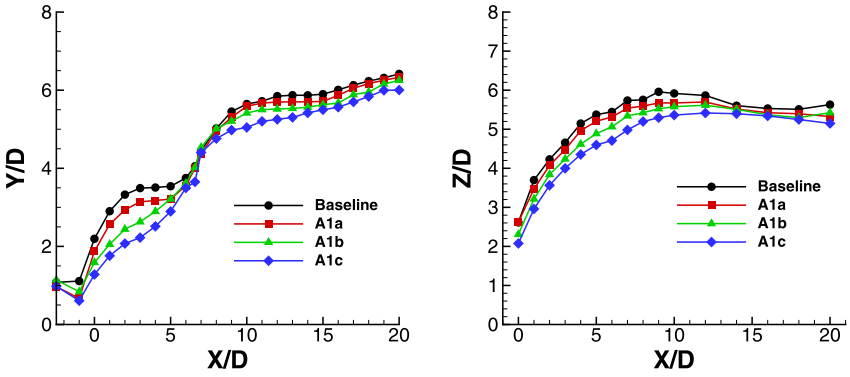

(a) Penetration (b) Spread

Fig. 9. Mixing characteristics for Case A1.

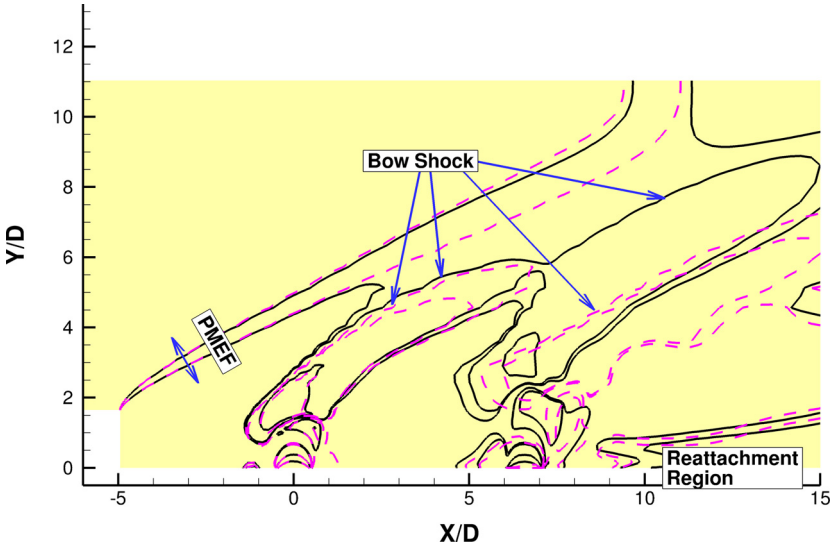

Fig. 10. Superposition of the isobars $P_{0,norm}$ of the baseline case (solid lines) and the case A2c (dashed lines).

Table 4
Case A1.

Case	Ω_{norm}	$\Delta\Omega$
Baseline	1	0
A1a	-0.905	-9.48%
A1b	0.811	-18.905%
A1c	0.763	-23.638%

flow. However, this effect is neutralized at the second injector which has an unchanged α and mass flow. Thus we see negligible effect in the streamwise vorticity beyond the second injector in Fig. 8a. Nevertheless, the entropy, stagnation pressure, penetration and spread are all affected even beyond the second injector. The entropy increase and the stagnation pressure loss is reduced, which means an improved thermodynamic performance. However, the penetration and spread are also reduced indicating lower mixing efficiency.

Table 4 shows the volume of mixing for different α for Case A1. In this table, Ω_{norm} is the ratio of volume of mixing of the case to the volume of mixing of the baseline (BL) case, and $\Delta\Omega$ is the percentage change in the volume of mixing with respect to the baseline case. From the table we see that as the angle of injection increases, the volume of mixing decreases.

We can conclude that increasing the α of the first injector, while keeping the second unchanged, has the effect of giving better thermodynamic performance at the cost of mixing efficiency.

Table 5
Case A2.

Section name	A2a	A2b	A3c
Injector 1	0°	0°	0°
Injector 2	15°	30°	45°

4.3.2. Case A2

For Case A2, the α for the 2nd injection is varied while the angle of the leading injector is kept unchanged at 0°. The different configurations for this case have been listed in Table 5.

Fig. 10 shows the imposition of isobars of Case A2c with the baseline case, while Fig. 11 and 12 show the comparison of the various flow properties for Case A2. As the α for the first injector is unchanged in this case, the bow shock structure for the first jet in Fig. 10 is essentially identical in both the cases, while significant difference is observed for the second jet. It can be observed from the figures, that all the flow properties follow the baseline results up to the 2nd jet after which they begin to deviate, in the near-field of the 2nd injector. As the streamwise momentum of the first jet remains unchanged there is no decrease in the shielding effect provided by the first jet. Increasing the α for the second jet results in increasing its streamwise momentum, resulting in the lower second peak of Γ_x, showing that the CRVs responsible for mixing have weakened in that region. The penetration height and spread of the second jet decreases significantly, as seen in Fig. 12. Figs. 11b and 11c show that the stagnation pressure loss and the

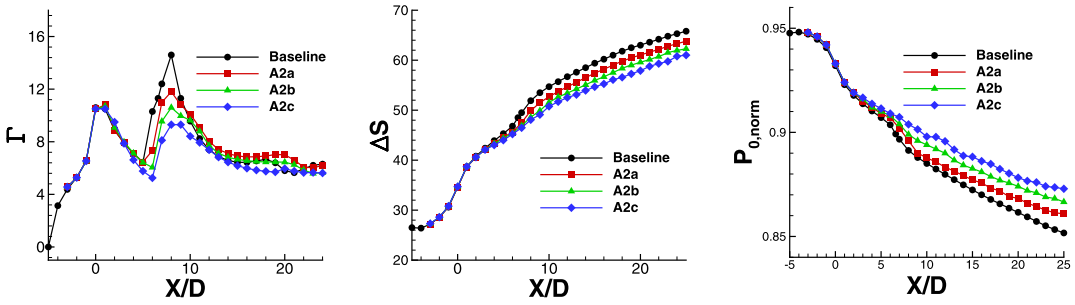

(a) Effect of Streamwise Vorticity (b) Entropy (c) Stagnation Pressure

Fig. 11. Flow characteristics for Case A2.

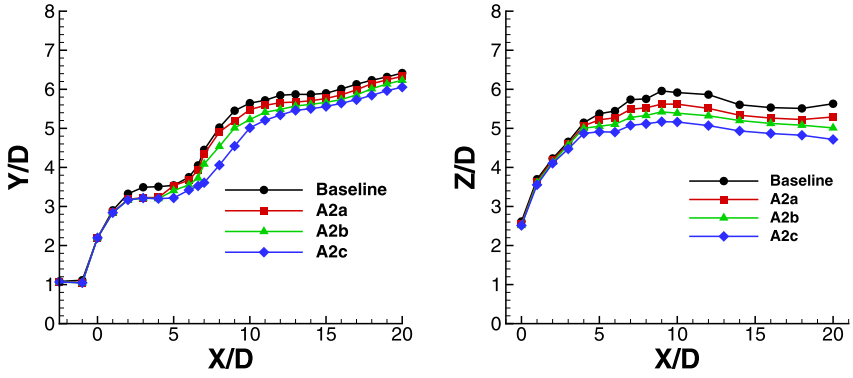

(a) Penetration (b) Spread

Fig. 12. Mixing characteristics for Case A2.

Table 6
Case A2.

Case	Ω_{norm}	$\Delta\Omega$
Baseline	1	0
A2a	0.905	-9.435%
A2b	0.758	-24.241%
A2c	0.620	-37.997%

Table 7
Case A3.

Section name	A3a	A3b	A3c
Injector 1	15°	30°	45°
Injector 2	15°	30°	45°

entropy increase both decrease from the near-field of 2nd injector, resulting in a thermodynamically more efficient system with increasing α. Table 6 shows the volume of mixing decreases with increase in α for the second jet.

Again we find that increasing α even in the second jet, with the first jet being unchanged, causes an increase in thermodynamic performance, but at the cost of decreased mixing.

4.3.3. Case A3

In Case A3, the angle of injection for both injectors is varied by the same amount. The different configurations are listed in Table 7.

In Fig. 13, the isobars for Case A3c have been superimposed with the baseline case, while the Figs. 14 and 15 shows the comparison of the various flow properties for Case A3. The bow-shock structures in Fig. 13 show significant difference between Case A3c and the baseline case for both the injectors. The streamwise momentum of both jets increase with increase in α. The reduced peak value of Γ_x for the first jet results weaker CRV with increase in α.

Table 8
Case A3.

Case	Ω_{norm}	$\Delta\Omega$
Baseline	1	0
A3a	0.830	-16.957%
A3b	0.661	-33.921%
A3c	0.421	-57.883%

As discussed in the earlier cases, weaker CRVs results in lesser jet spread and penetration. The reduced shielding effect by the first jet in addition to its increased streamwise momentum leads to the decrease in the peak value of Γ_x for second injector with increase in αs as seen in Fig. 14a. The two peaks of Γ_x in Fig. 14a become quite similar with significant decrease in jet penetration and spread, even to the extent of the eradication, as seen in Fig. 15a, of the mixing augmentation bump in the penetration at the 2nd injector seen in previous cases. The decrease in entropy rise and stagnation pressure loss, as seen in Fig. 14b and 14c, makes the system with higher α thermodynamically more efficient, but the purpose of having multiple injectors to augment mixing is not fulfilled. These results indicate that such configurations do not lead to any meaningful gain in the performance. Table 8 shows the volume of mixing for Case A3, which shows that the mixing drastically reduces with increase in α.

4.4. Case B: α variation between $-45°$ and $0°$

In case B, the effect of slanting the jets in the direction opposite to the incoming cross-flow (hence the negative sign) is studied. The α for various injectors is varied between $0°$ and $-45°$, resulting in various combinations that are grouped into several sub-cases. At the end of this section, the flow features between the different sub-cases and the baseline case are compared.

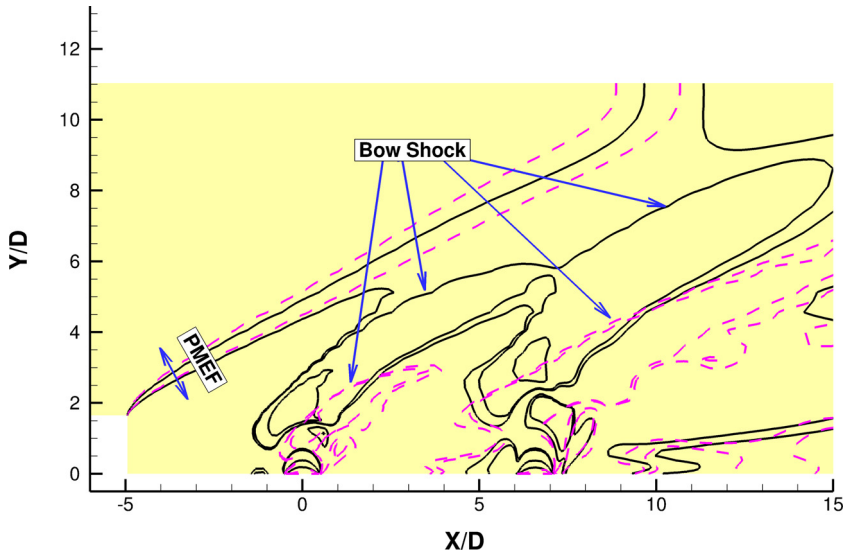

Fig. 13. Superposition of the isobars $P_{0,norm}$ of the baseline case (solid lines) and the case A3c (dashed lines).

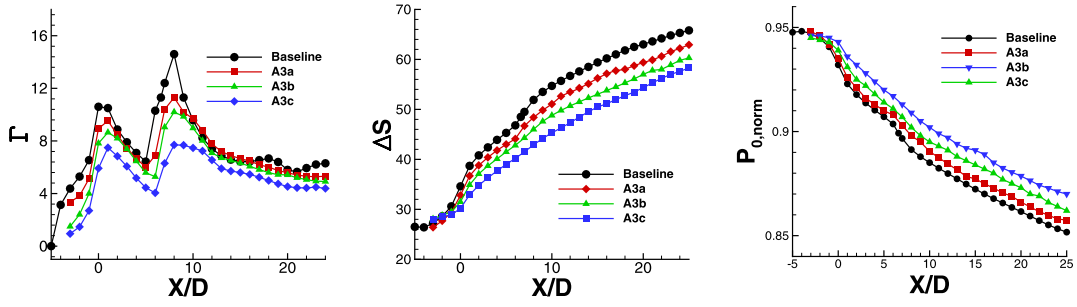

(a) Effect of Streamwise Vorticity (b) Entropy (c) Stagnation Pressure

Fig. 14. Flow characteristics for Case A3.

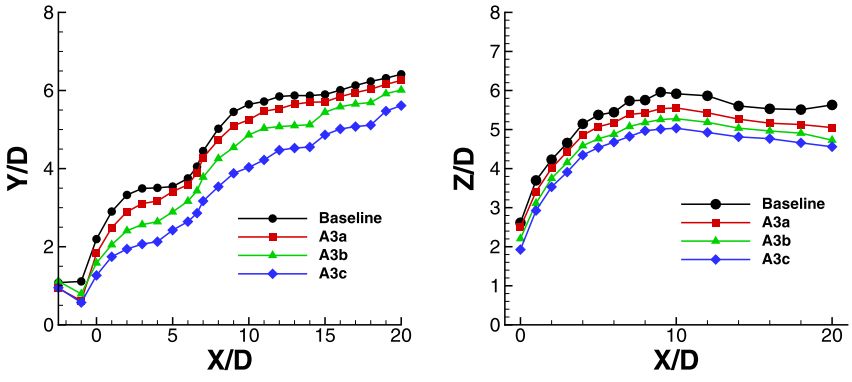

(a) Penetration (b) Spread

Fig. 15. Mixing characteristics for Case A3.

4.4.1. Case B1

In this case, the α of the first injector is varied in the direction opposite to the incoming cross-flow, while keeping the α of the second injector at 0°. The different configurations studied in this case are listed in Table 9. Fig. 16 shows the imposition of the isobars of Case B1c with the baseline case, while Figs. 17 and 18 show the comparison of the various flow properties for Case B1.

As the α of the first jet increases from 0° to −45°, its bow shock bends towards the step, which increases the bow shock impingement on the Prandtl Meyer Expansion Fan (PMEF). The location of the reattachment shock and the barrel shock for the second jet remains the same. So the shock structure for the second jet largely remains unchanged. A small change is observed in the region above the shielding zone created by the first jet, which is due to the high momentum of the streamwise flow.

Table 9
Case B1.

Section name	B1a	B1b	B1c
Injector 1	−15°	−30°	−45°
Injector 2	0°	0°	0°

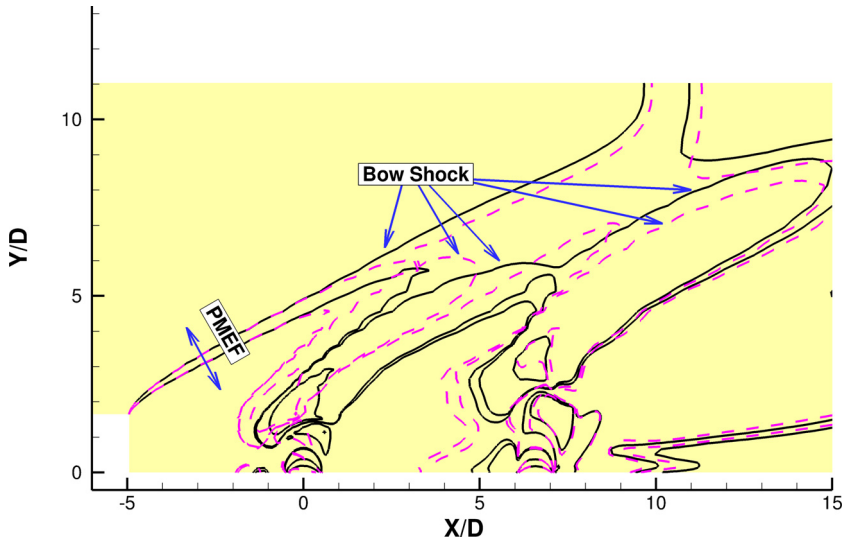

Fig. 16. Superposition of the isobars $P_{0,norm}$ of the baseline case (solid lines) and the case B1c (dashed lines).

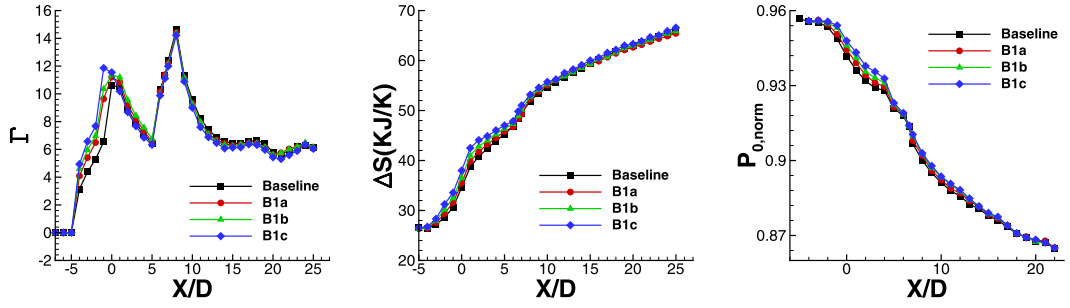

(a) Effect of Streamwise Vorticity (b) Entropy (c) Stagnation Pressure

Fig. 17. Flow characteristics for Case B1.

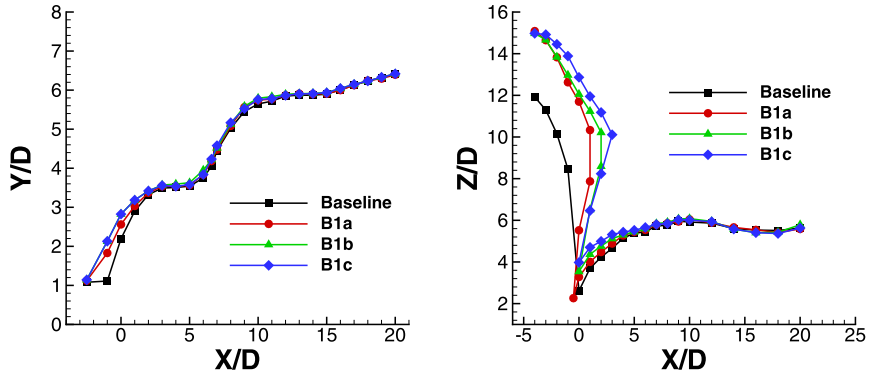

(a) Penetration (b) Spread

Fig. 18. Mixing characteristics for Case B1.

The first jet in the baseline case is located at the stagnation point created by the recirculation region due to the step. As the jet is injected in the direction opposite to the incoming flow, it encounters the recirculation zone, which results in the jet penetrating into it. This increases the penetration and spread of the fuel inside the recirculation zone. This penetration of the jet into the recirculation zone increases with increasing magnitude of α as seen in Fig. 18, resulting in a wider spread and higher penetration height in the immediate upstream of the jet.

Injecting the jet at a negative angle increases its streamwise momentum in the direction opposite to the incoming flow. Hence, an overall reduction in the streamwise momentum of the flow at the region near the first injector takes place. Therefore, a slight increase in Γ and thereby in the counter rotating vortices (CRV) can be observed at the jet inlet in Fig. 17a, which results in a nominal increase in the mixing and thermodynamic characteristics in this region. The streamwise momentum of the incoming flow then recovers in the region $X/D > 3$, which is in the downstream of the first jet. Therefore, it can be observed from Fig. 17 and 18, that the thermodynamic and the mixing characteristics remain the same as the baseline case in the region beyond $X/D > 3$. It maybe noted that Fig. 18b shows multiple values of spread for values of

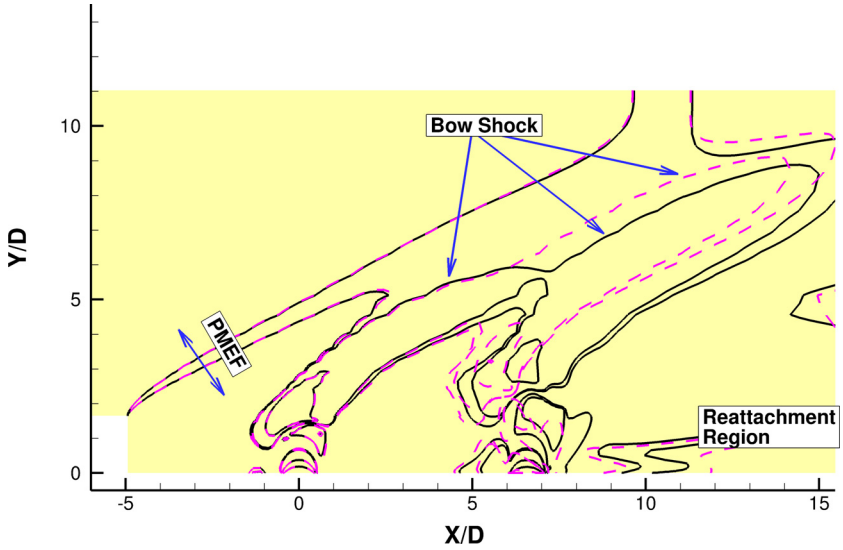

Fig. 19. Superposition of the isobars $P_{0,norm}$ of the baseline case (solid lines) and the case B2c (dashed lines).

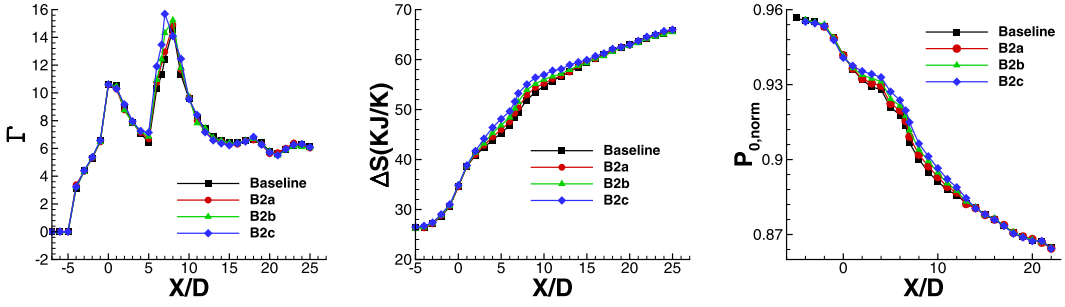

(a) Effect of Streamwise Vorticity (b) Entropy (c) Stagnation Pressure

Fig. 20. Flow characteristics for Case B2.

Table 10
Case B1.

Case	Ω_{norm}	$\Delta\Omega$
Baseline	1	0
B1a	1.063	6.320%
B1b	1.070	7.035%
B1c	1.084	8.428%

Table 11
Case B2.

Section name	B2a	B2b	B3c
Injector 1	0°	0°	0°
Injector 2	−15°	−30°	−45°

X/D around the first injector. This is because the spread in this case occurs both in the recirculation zone as well as above it, in the cross-flow. The scalar that is diffused into the recirculation zone gets spread throughout its width and is shown by the vertical branch of the plot, while the spread in the crossflow is shown in the horizontal branch. Table 10 shows the volume of mixing for different α for Case B1. From the table we see that as the angle of injection increases, the volume of mixing increases. It should however be noted that, with increase in α, more fuel is being trapped in the recirculation zone, which also acts as a flame-holder. We can conclude that increasing the α of the first injector in the direction opposing the crossflow, while keeping the second unchanged, results in better flame-holding, while giving the same thermodynamic performance as the baseline case (see Fig. 16).

4.4.2. Case B2

For Case B2, the α for the leading injector is maintained at 0°, while the 2nd injection is varied opposite to the direction of the incoming high-speed flow. The different configurations for this case have been listed in Table 11. Fig. 19 shows the imposition of isobars of Case B2 with the baseline case, while Fig. 20 and 21 show the comparison of the various flow properties for Case B2. The bow shock structure for the first jet in Fig. 19 is essentially identical to the baseline case, as the α for the first injector is unchanged, while significant difference is observed for the second jet. It can be observed from the figures, that all the flow properties follow the baseline results up to the transition region at $X/D \approx 4$, after which they begin to deviate. The shielding effect provided by the first jet remains unchanged as the streamwise momentum of the first jet remains unchanged.

Increasing α for the second jet results in increasing its streamwise momentum in the direction opposing the incoming flow. This changes the second bow-shock, resulting in more flow blockage in the region between the two jets. This reduces the streamwise overall momentum the upstream of the injector, increasing the shielding effect, and thereby increasing the fuel residence time in the combustor. There is an increase in peak Γ_x, due to the negative angle of injection, resulting in stronger CRVs at the second injector. The flow properties begin to deviate as early as the beginning of the transition zone from $X/D \approx 4$ as seen in Figs. 20 and 21. Table 12 shows the volume of mixing increases slightly with increase in negative α for the second jet. In this case, the volume

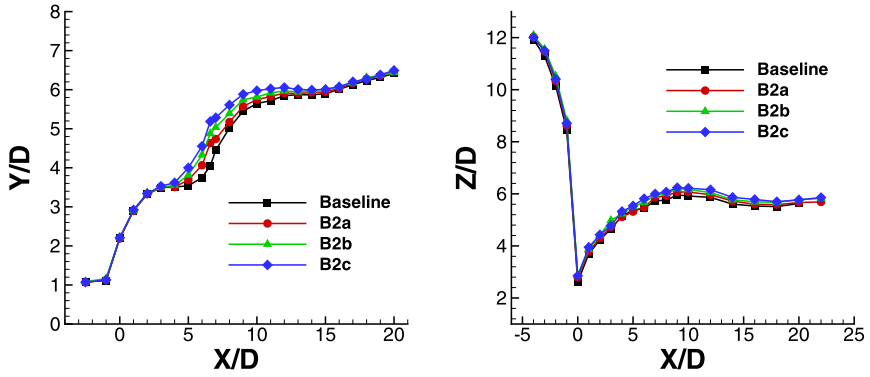

(a) Penetration (b) Spread

Fig. 21. Mixing characteristics for Case B2.

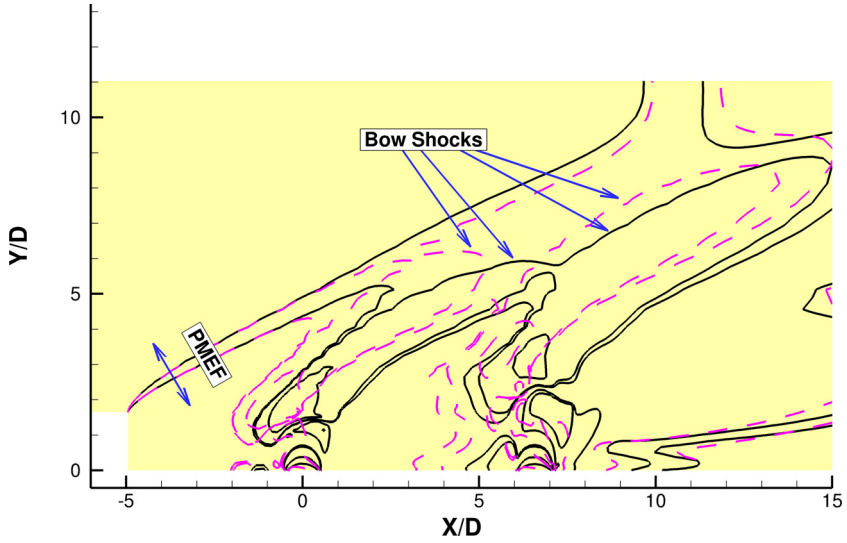

Fig. 22. Superposition of the isobars $P_{0,norm}$ of the baseline case (solid lines) and the case B3c (dashed lines).

Table 12
Case B2.

Case	Ω_{norm}	$\Delta\Omega$
Baseline	1	0
B2a	1.003	0.327%
B2b	1.009	0.943%
B2c	1.011	1.197%

Table 13
Case B3.

Section name	B3a	B3b	B3c
Injector 1	−15°	−30°	−45°
Injector 2	−15°	−30°	−45°

of mixing increases inside the combustor, unlike the Case B1, as the injector is situated away from the recirculation zone. Therefore the amount of fuel available for combustion increases inside the combustor, although nominally, resulting in a nominally better mixing augmentation than the baseline case. But like in the previous cases, the increase in air-fuel mixing augmentation comes with almost no thermodynamic penalty.

4.4.3. Case B3

In this case, the angles of injection are varied by the same amount for both jets in the opposite direction to the incoming cross-flow. Table 13 lists the different configurations considered in Case B3. Fig. 22 shows the imposition of isobars of Case B3 with the baseline case, while Fig. 23 and 24 show the comparison of the various flow properties for Case B3. The bow-shock structures in Fig. 22 bend towards the step and show significant difference between Case B3c and the baseline case for both the injectors. The increased peak value of Γ_x for the first jet results stronger CRV with increase in negative α. As discussed in the earlier cases, stronger CRVs results in more jet spread and penetration. The increased shielding effect by the first jet in addition to the decreased streamwise momentum of the incoming flow leads to the increase in the peak value of Γ_x for second injector with increase in negative α as seen in Fig. 23a. Therefore, mixing is augmented at both injectors, while the final entropy rise and stagnation pressure loss as seen in Figs. 23b and 23c remains same. In the region around the second injector, the penetration and spread again increases, due to increased shielding effect, as discussed earlier. This results in a significant increase in volume of mixing is noted as compared to any of the previous cases and the baseline case.

Table 14 shows the volume of mixing for Case B3, which shows that the mixing is augmented significantly for all negative α. More fuel is trapped in the recirculation zone with increasing negative α, making it richer in fuel and increasing the ease of flame-holding. It is also seen that the increased mixing comes with almost no thermodynamic penalty. These results indicate that such negative α configuration result in a significant gain in the performance.

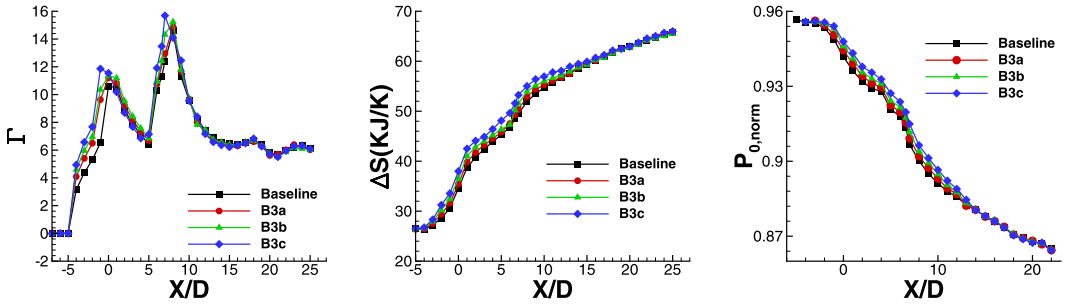

(a) Effect of Streamwise Vorticity (b) Entropy (c) Stagnation Pressure

Fig. 23. Flow characteristics for Case B3.

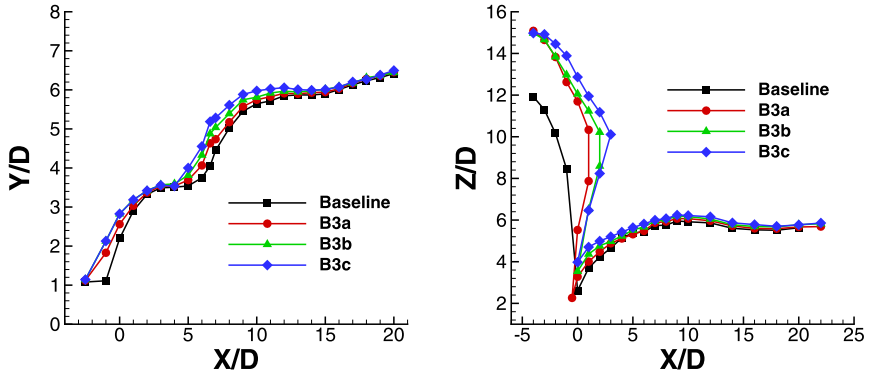

(a) Penetration (b) Spread

Fig. 24. Mixing characteristics for Case B3.

Table 14
Case B3.

Case	Ω_{norm}	$\Delta\Omega$
Baseline	1	0
B3a	1.107	10.731%
B3b	1.112	11.265%
B3c	1.124	12.4%

5. Conclusions

The effect of variation of angle of injections in a multi injector SCRAMJET engine has been studied in detail in this paper using the low-Re SST model Menter's SST model on an in-house 3-D unstructured solver. Two cases have been formed on the basis of direction of the angle of injection. Case A varies the injection in the streamwise direction of the flow, while Case B varies the injection angle in the direction opposing to the incoming flow. Three sub-cases have been formed in each case with combinations of the angle of injection of the two jets and the results are compared with the baseline case.

In Case A, we see that as the angle of injection are increased, we get better thermodynamic performance but at the cost of severely decreased mixing volumes. In case B, we see that mixing volume is significantly increased, particularly where both jets have the same (negative) angles of injection, with almost no thermodynamic penalty. Interestingly, the mixing enhancement is only slightly affected for $-15°$, $-30°$ and $-45°$, with more negative angles being better. However, with higher negative α's there is more penetration of the fuel into the recirculation zone, which could enhance flame-holding but also cause fuel loss. Therefore the conclusion that this study leads us to is that the injection angles of both jets be slanted *opposing* the inflow by as much as 45° to get better flame-holding and enhanced mixing at no cost to thermodynamic performance. This conclusion is very interesting as there has been no suggestion in the research literature, to the best of the authors knowledge, that negative angles of injection would be advantageous to the SCRAMJET's performance.

6. Funding

This research did not receive any specific grant from funding agencies in public, commercial or not-for-profit sectors.

Declaration of competing interest

The authors declare that they have no known competing financial interests or personal relationships that could have appeared to influence the work reported in this paper.

References

[1] P. Roncioni, P. Natale, M. Marini, T. Langener, J. Steelant, Numerical simulations and performance assessment of a scramjet powered cruise vehicle at Mach 8, Aerosp. Sci. Technol. 42 (2015) 218–228, https://doi.org/10.1016/j.ast.2015.01.006.

[2] S. Chen, D. Zhao, Rans investigation of the effect of pulsed fuel injection on scramjet hyshot ii engine, Aerosp. Sci. Technol. 84 (2019) 182–192, https://doi.org/10.1016/j.ast.2018.10.022.

[3] S. Aso, S. Okuyama, Y. Ando, T. Fujimori, Two-dimensional and three-dimensional mixing flow fields in supersonic flow induced by injected secondary flows through traverse slot and circular nozzle, in: 31st Aerospace Sciences Meeting, AIAA, Reno, NV, U.S.A., 1993, p. 489.

[4] W. Huang, L. Yan, Progress in research on mixing techniques for transverse injection flow fields in supersonic crossflows, J. Zhejiang Univ. Sci. A 14 (8) (2013) 554–564, https://doi.org/10.1631/jzus.A1300096.

[5] W. Huang, Transverse jet in supersonic crossflows, Aerosp. Sci. Technol. 50 (2016) 183–195, https://doi.org/10.1016/j.ast.2016.01.001.

[6] W. Huang, Y. Li, L. Yan, R. Moradi, Mixing enhancement mechanism induced by the cascaded fuel injectors in supersonic flows: a numerical study, Acta Astronaut. 152 (2018) 18–26, https://doi.org/10.1016/j.actaastro.2018.07.027.
[7] K. Arora, K. Chakravarthy, D. Chakraborty, Large eddy simulation of supersonic, compressible, turbulent mixing layers, Aerosp. Sci. Technol. 86 (2019) 592–598, https://doi.org/10.1016/j.ast.2019.01.034.
[8] L.-q. Li, W. Huang, L. Yan, Z.-b. Du, M. Fang, Numerical investigation and optimization on the micro-ramp vortex generator within scramjet combustors with the transverse hydrogen jet, Aerosp. Sci. Technol. 84 (2019) 570–584, https://doi.org/10.1016/j.ast.2018.11.011.
[9] J.C. McDaniel, J. Raves, Laser-induced-fluorescence visualization of transverse gaseous injection in a nonreacting supersonic combustor, J. Propuls. Power 4 (6) (1988) 591–597, https://doi.org/10.2514/3.23105.
[10] J. Mcdaniel, D. Fletcher, R. Hartfield, S. Hollo, Transverse Injection into Mach 2 Flow Behind a Rearward-Facing Step – A 3-D, Compressible Flow Test Case for Hypersonic Combustor CFD Validation, AIAA, 1991, p. 5071.
[11] A. Karagozian, K. Wang, A.-T. Le, O. Smith, Transverse gas jet injection behind a rearward-facing step, J. Propuls. Power 12 (6) (1996) 1129–1136, https://doi.org/10.2514/3.24153.
[12] D. Chakraborty, A. Roychowdhury, V. Ashok, P. Kumar, Numerical investigation of staged transverse sonic injection in Mach 2 stream in confined environment, Aeronaut. J. 107 (1078) (2003) 719–729, https://doi.org/10.1017/S0001924000013476.
[13] A. Sriram, D. Chakraborty, Numerical exploration of staged transverse injection into confined supersonic, Def. Sci. J. 61 (1) (2011) 3–11, https://doi.org/10.14429/dsj.61.20.
[14] V. Ton, A. Karagozian, F. Marble, S. Osher, B. Engquist, Numerical simulations of high-speed chemically reacting flow, Theor. Comput. Fluid Dyn. 6 (2–3) (1994) 161–179, https://doi.org/10.1007/BF00312347.
[15] S.-H. Lee, I.-S. Jeung, Y. Yoon, Computational investigation of shock-enhanced mixing and combustion, AIAA J. 35 (12) (1997) 1813–1820, https://doi.org/10.2514/2.56.
[16] S.-H. Lee, I.-S. Jeung, Y. Yoon, Computational investigation of shock-enhanced mixing: application to circular cross section combustor, AIAA J. 36 (11) (1998) 2055–2062, https://doi.org/10.2514/2.306.
[17] V. Sharma, V. Eswaran, D. Chakraborty, Effect of location of a transverse sonic jet on shock augmented mixing in a scramjet engine, Aerosp. Sci. Technol. 96 (2020) 105535, https://doi.org/10.1016/j.ast.2019.105535.
[18] V. Sharma, V. Eswaran, D. Chakraborty, Determination of optimal spacing between transverse jets in a scramjet engine, Aerosp. Sci. Technol. 96 (2020) 105520, https://doi.org/10.1016/j.ast.2019.105520.
[19] R. Mays, R. Thomas, J. Schetz, Low angle injection into a supersonic flow, in: 25th Joint Propulsion Conference, 1989, p. 2461.
[20] E. Fuller, R. Mays, R. Thomas, J. Schetz, Mixing studies of helium in air at high supersonic speeds, AIAA J. 30 (9) (1992) 2234–2243, https://doi.org/10.2514/3.11210.
[21] S. Aso, K. Inoue, K. Yamaguchi, Y. Tani, A study on supersonic mixing by circular nozzle with various injection angles for air breathing engine, Acta Astronaut. 65 (5–6) (2009) 687–695, https://doi.org/10.1016/j.actaastro.2009.01.051.
[22] M. Gruber, A. Nejadt, T. Chen, J.C. Dutton, Mixing and penetration studies of sonic jets in a Mach 2 freestream, J. Propuls. Power 11 (2) (1995) 315–323, https://doi.org/10.2514/3.51427.
[23] E. Jeong, I.-S. Jeung, S. O'Byrne, A.P. Houwing, Investigation of supersonic combustion with angled injection in a cavity-based combustor, J. Propuls. Power 24 (6) (2008) 1258–1268, https://doi.org/10.2514/1.36519.
[24] H. Wang, Z. Wang, M. Sun, N. Qin, Simulations of combustion with normal and angled hydrogen injection in a cavity-based supersonic combustor, Proc. Inst. Mech. Eng., G J. Aerosp. Eng. 228 (4) (2014) 530–541, https://doi.org/10.1177/0954410013475567.
[25] W. Huang, L. Ma, M. Pourkashanian, D. Ingham, S. Luo, Z. Wang, Parametric effects in a scramjet engine on the interaction between the air stream and the injection, Proc. Inst. Mech. Eng., G J. Aerosp. Eng. 226 (3) (2012) 294–309, https://doi.org/10.1177/0954410011408512.
[26] Y. Zhang, W. Liu, B. Wang, Effects of oblique and transverse injection on the characteristics of jet in supersonic crossflow, Acta Astronaut. 115 (2015) 356–366, https://doi.org/10.1016/j.actaastro.2015.06.004.
[27] V. Sharma, V. Eswaran, D. Chakraborty, Computational analysis of transverse sonic injection in supersonic crossflow using rans models, J. Fluids Eng. (2020), https://doi.org/10.1115/1.4045985.
[28] J.M. Weiss, W.A. Smith, Preconditioning applied to variable and constant density flows, AIAA J. 33 (11) (1995) 2050–2057, https://doi.org/10.2514/3.12946.
[29] P.L. Roe, Approximate Riemann solvers, parameter vectors, and difference schemes, J. Comput. Phys. 43 (2) (1981) 357–372, https://doi.org/10.1016/0021-9991(81)90128-5.
[30] J.M. Weiss, J.P. Maruszewski, W.A. Smith, Implicit solution of preconditioned Navier-Stokes equations using algebraic multigrid, AIAA J. 37 (1) (1999) 29–36, https://doi.org/10.2514/2.689.
[31] V. Venkatakrishnan, On the accuracy of limiters and convergence to steady state solutions, in: 31st Aerospace Sciences Meeting, AIAA, Reno, NV, U.S.A., 1993, p. 880.
[32] V. Venkatakrishnan, Convergence to steady state solutions of the Euler equations on unstructured grids with limiters, J. Comput. Phys. 118 (1) (1995) 120–130, https://doi.org/10.1006/jcph.1995.1084.
[33] J. Lynn, Multigrid solution of the Euler equations with local preconditioning.
[34] F.R. Menter, Two-equation eddy-viscosity turbulence models for engineering applications, AIAA J. 32 (8) (1994) 1598–1605, https://doi.org/10.2514/3.12149.
[35] P.J. Roache, Perspective: a method for uniform reporting of grid refinement studies, J. Fluids Eng. 116 (3) (1994), https://doi.org/10.1115/1.2910291.